

# A comparison of different order hybrid finite difference-volume methods for solving the Serre equations in conservative law form

Jordan Pitt,<sup>1</sup>  
Christopher Zoppou,<sup>1</sup>  
Stephen G. Roberts,<sup>1</sup>

## ABSTRACT

In this paper first-, second- and third-order accurate numerical methods for solving the Serre equations are described. The method is described as a finite difference-volume method because it uses a finite difference approximation and a finite volume method to solve the Serre equations in conservation law form. These models are validated and used to investigate a conjecture in the literature about the results of solving the Serre equations in the presence of steep gradients. To adequately resolve dispersive waves efficiently in problems containing steep gradients a scheme is required to be at least a second-order accurate.

**Keywords:** dispersive waves, conservation laws, Serre equations, finite volume method, finite difference method

## <sup>1</sup> INTRODUCTION

Free surface flows occur in many important applications such as; tsunamis, storm surges and tidal bores. Because fluid viscosity has a negligible effect on these problems they can be modelled by the Euler equations. However, numerical methods for the Euler equations are not yet computationally efficient enough to deal with these problems over large domains. Thus various approximations to the Euler equations have been derived, one of the crudest is the shallow water wave (SWW) equations which have been used to model free surface flows in the past. However, the SWW equations assume a hydrostatic pressure distribution in a fluid column which is not fully justified in rapidly varying flows

---

<sup>1</sup>Mathematical Sciences Institute, Australian National University, Canberra, ACT 0200, Australia, E-mail: Jordan.Pitt@anu.edu.au. The work undertaken by the first author was supported financially by an Australian National University Scholarship.

10 because vertical acceleration of the fluid particles becomes important. It is the vertical  
11 acceleration of these particles that produces a non-hydrostatic pressure distribution and  
12 dispersive waves which are not present in the SWW equations. Consequently, many equa-  
13 tions have been derived as approximations to the Euler equations in shallow fluids that are  
14 less restrictive in their assumptions than the SWW equations. The Serre equations are one  
15 of these approximations to the Euler equations and are of particular interest because they  
16 do not enforce a hydrostatic pressure distribution over a fluid column allowing for fully  
17 non-linear and weakly dispersive flows (Lannes and Bonneton 2009).

18 The Serre equations were first derived by Serre (1953) for flat bottom topographies in  
19 one dimension. More general equations were then derived for smooth bottom topographies  
20 in one dimension (Su and Gardner 1969) and later smooth bottom topographies in two di-  
21 mensions (Green and Naghdi 1976). These equations have been handled in many different  
22 ways (Mitsotakis et al. 2014; Bonneton et al. 2011; Antunes do Carmo et al. 1993; Chazel  
23 et al. 2011; Cienfuegos and Bonneton 2006; Cienfuegos and Bonneton 2007; Dutykh et al.  
24 2011). This paper follows the decomposition of the Serre equations into conservative law  
25 form (Le Métayer et al. 2010; Li et al. 2014; Zoppou 2014) and follows the formulation  
26 of Le Métayer et al. (2010) and Zoppou (2014). First-, second- and third-order accurate  
27 numerical methods are developed for solving the Serre equations in conservation law form.

28 Zoppou and Roberts (1996) demonstrated that first- and third-order methods produce  
29 diffusive errors smearing steep gradients. While second-order methods produce dissipative  
30 errors introducing non-physical oscillations around steep gradients. Because steep  
31 gradients arise naturally in fluid flows and the Serre equations produce dispersive waves  
32 (El et al. 2006) it is important that physical oscillations described by the dispersive terms  
33 are not significantly polluted by either diffusion or dissipation.

34 This paper aims to clear up the discrepancy between the results of Le Métayer et al.  
35 (2010) and El et al. (2006) by examining the behaviour of a certain dam-break problem.  
36 In particular, Le Métayer et al. (2010) stated that their first-order method was sufficient to  
37 capture the important behaviour of the dam-break problem, this paper will test the validity  
38 of that assertion. To accomplish this first-, second- and third-order accurate methods to  
39 solve the Serre equations are constructed and validated by comparing the solutions to a  
40 known analytical solution to the Serre equations and laboratory data of flows containing  
41 steep gradients. Then the validated models are used to resolve this conflict.

## 42 SERRE EQUATIONS

43 The Serre equations can be derived by integrating the Euler equations over the water  
44 depth, as was done by Su and Gardner (1969). They can also be derived from an asymptotic  
45 expansion of the Euler equations (Lannes and Bonneton 2009). The former is more  
46 consistent with the perspective from which numerical methods will be developed in this

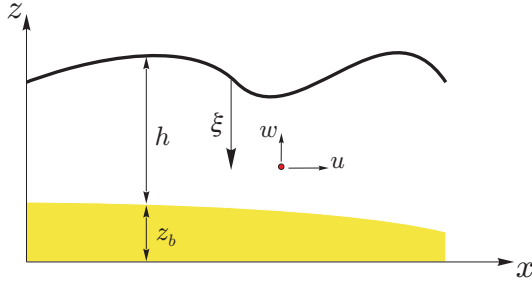


FIG. 1: The notation used for one-dimensional flow governed by the Serre equation.

47 paper while the latter is useful for identifying the appropriate regions in which to use these  
 48 equations as a model of fluid flow.

49 The scenario under which the Serre approximation is made consists of a two dimensional  
 50  $\mathbf{x} = (x, z)$  fluid over a variable bathymetry as in Figure 1, under the action of  
 51 gravity. The water depth is  $h(x, t)$  and  $z_b(x)$  is the bed elevation. The fluid is subject  
 52 to the pressure,  $p(\mathbf{x}, t)$  and gravitational acceleration,  $\mathbf{g} = (0, g)^T$  and has a velocity  
 53  $\mathbf{v} = (u(\mathbf{x}, t), w(\mathbf{x}, t))$ , where  $u(\mathbf{x}, t)$  is the velocity in the  $x$ -coordinate and  $w(\mathbf{x}, t)$  is the  
 54 velocity in the  $z$ -coordinate and  $t$  is time. Assuming that  $z_b(x)$  is constant the Serre equa-  
 55 tions read (Li et al. 2014; Zoppou 2014)

$$56 \quad \frac{\partial h}{\partial t} + \frac{\partial(\bar{u}h)}{\partial x} = 0, \quad (1a)$$

57

58

$$59 \quad \underbrace{\frac{\partial(\bar{u}h)}{\partial t} + \frac{\partial}{\partial x} \left( \bar{u}^2 h + \frac{gh^2}{2} \right)}_{\text{Shallow Water Wave Equations}} + \underbrace{\frac{\partial}{\partial x} \left( \frac{h^3}{3} \left[ \frac{\partial \bar{u}}{\partial x} \frac{\partial \bar{u}}{\partial x} - \bar{u} \frac{\partial^2 \bar{u}}{\partial x^2} - \frac{\partial^2 \bar{u}}{\partial x \partial t} \right] \right)}_{\text{Dispersion Terms}} = 0 \quad (1b)$$

60

61 where  $\bar{u}$  is the depth averaged velocity.

## 62 Alternative Conservation Law Form of the Serre Equations

63 In Le Métayer et al. (2010) and Zoppou (2014) it is demonstrated that the Serre equa-  
 64 tions can be rearranged into a conservation law form, by introducing a new conserved  
 65 quantity

$$66 \quad G = uh - h^2 \frac{\partial h}{\partial x} \frac{\partial u}{\partial x} - \frac{h^3}{3} \frac{\partial^2 u}{\partial x^2}. \quad (2)$$

67

68 Consequently, (1) can be rewritten as

$$69 \quad 70 \quad \frac{\partial h}{\partial t} + \frac{\partial(uh)}{\partial x} = 0 \quad (3a)$$

71 and

$$72 \quad 73 \quad \frac{\partial G}{\partial t} + \frac{\partial}{\partial x} \left( Gu + \frac{gh^2}{2} - \frac{2h^3}{3} \frac{\partial u}{\partial x} \frac{\partial u}{\partial x} \right) = 0 \quad (3b)$$

74 where the bar over  $u$  has been dropped to simplify the notation. A hybrid method can be  
 75 developed for the Serre equations that solves the elliptic problem (2) for  $u$  and then the  
 76 conservation law (3) for  $h$  and  $G$ . This replicates the process of Le Métayer et al. (2010)  
 77 and Zoppou (2014).

## 78 NUMERICALLY SOLVING THE SERRE EQUATIONS WRITTEN IN 79 CONSERVATION LAW FORM

80 There are numerous ways a numerical method could be built to solve the Serre equa-  
 81 tions in conservation law form (3). For flows that contain steep gradients the finite volume  
 82 method seems the most appropriate. A finite volume method to solve (3) updates the  
 83 conserved quantities  $h$  and  $G$  over a single time step  $\Delta t = t^{n+1} - t^n$ . So that

$$84 \quad 85 \quad \begin{bmatrix} h^{n+1} \\ G^{n+1} \end{bmatrix} = \mathcal{L}(h^n, G^n, u^n, \Delta t) \quad (4)$$

86 where  $\mathcal{L}$  is some numerical solver for (3) and the superscript denotes the time at which a  
 87 quantity is evaluated; e.g.  $u^n = u(t^n)$ . The complete solution also involves solving (2) for  
 88  $u$  given  $h$  and  $G$  denoted by

$$88 \quad u^{n+1} = \mathcal{A}(h^{n+1}, G^{n+1}). \quad (5)$$

91

## 92 SOLVING THE ELLIPTIC EQUATION $\mathcal{A}$ FOR $U$

93 Assuming that a discretisation in space has a fixed resolution so that  $\forall i x_{i+1} - x_i =$   
 94  $\Delta x$ ; allows for a simple finite difference approximation to (2) as a suitable method for  
 95  $\mathcal{A}$  (Le Métayer et al. 2010; Zoppou 2014). Since the goal of this paper is to develop  
 96 and compare a range of different order accurate methods for this problem both a second-  
 97 and fourth-order centred finite difference approximation to (2) were used. By taking such  
 98 approximations to the first- and second-order spatial derivatives the second- and fourth-  
 99 order analogues of (2) are given by

$$100 \quad 101 \quad G_i = u_i h_i - h_i^2 \left( \frac{h_{i+1} - h_{i-1}}{2\Delta x} \right) \left( \frac{u_{i+1} - u_{i-1}}{2\Delta x} \right) - \frac{h_i^3}{3} \left( \frac{u_{i+1} - 2u_i + u_{i-1}}{\Delta x^2} \right) \quad (5a)$$

102 and

$$G_i = u_i h_i - h_i^2 \left( \frac{-h_{i+2} + 8h_{i+1} - 8h_{i-1} + h_{i-2}}{12\Delta x} \right) \left( \frac{-u_{i+2} + 8u_{i+1} - 8u_{i-1} + u_{i-2}}{12\Delta x} \right) - \frac{h_i^3}{3} \left( \frac{-u_{i+2} + 16u_{i+1} - 30u_i + 16u_{i-1} - u_{i-2}}{12\Delta x^2} \right) \quad (5b)$$

105 where the subscript denotes the spatial coordinate at which the quantity is evaluated; e.g.  
 106  $u_i = u(x_i)$ . Both of these can be rearranged into a matrix equation with the following form

$$\begin{bmatrix} u_0 \\ \vdots \\ u_m \end{bmatrix} = A^{-1}(h) \begin{bmatrix} G_0 \\ \vdots \\ G_m \end{bmatrix} =: \mathcal{A}(h, G)$$

where for a second-order approximation the matrix  $A(h)$  is tri-diagonal while for a fourth-order method it is penta-diagonal.

# 111 SOLVING THE CONSERVATION LAW FORM OF THE SERRE EQUATIONS

112 A finite volume method of sufficient order was developed to solve (3). Unlike finite  
 113 difference methods which utilise nodal values of quantities, finite volume methods use the  
 114 cell averages, for example the average water depth over a cell which spans  $[x_{i-1/2}, x_{i+1/2}]$   
 115 is

$$\bar{h}_i = \frac{1}{\Delta x} \int_{x_{i-\frac{1}{2}}}^{x_{i+\frac{1}{2}}} h(x, t) dx$$

118 where  $x_{i \pm 1/2} = x_i \pm \Delta x/2$ . Finite volume methods update the cell averages using

$$U_i^{n+1} = U_i^n - \frac{\Delta t}{\Delta x} \left( F_{i+\frac{1}{2}}^n - F_{i-\frac{1}{2}}^n \right) \quad (6)$$

where  $\bar{U}_i^n = [\bar{h}_i^n \ \bar{G}_i^n]^T$  is an approximation of the vector of the conserved quantities averaged over the cell at time  $t^n$ . While  $F_{i\pm 1/2}^n$  is an approximation of the average flux over the time interval  $[t^n, t^{n+1}]$  at the respective cell boundary  $x_{i\pm 1/2}$ , which is obtained by solving a local Riemann problem at the cell boundaries.

125 Local Riemann Problem

Since  $\bar{U}_i^n$  is known for all  $i$  what remains is to calculate the time averaged fluxes  $F_{i\pm 1/2}$  in (6). In Kurganov et al. (2002) the time averaged inter-cell flux is approximated by

$$F_{i+\frac{1}{2}} = \frac{a_{i+\frac{1}{2}}^+ f(q_{i+\frac{1}{2}}^-) - a_{i+\frac{1}{2}}^- f(q_{i+\frac{1}{2}}^+)}{a_{i+\frac{1}{2}}^+ - a_{i+\frac{1}{2}}^-} + \frac{a_{i+\frac{1}{2}}^+ a_{i+\frac{1}{2}}^-}{a_{i+\frac{1}{2}}^+ - a_{i+\frac{1}{2}}^-} \left[ q_{i+\frac{1}{2}}^+ - q_{i+\frac{1}{2}}^- \right] \quad (7)$$

130 where  $f$  is the instantaneous flux of the conserved quantity  $q$  evaluated using the recon-  
 131 structed values from the cells adjacent to the cell interface  $x_{i+1/2}$ . While  $a_{i+1/2}^-$  and  $a_{i+1/2}^+$   
 132 are given by

$$133 \quad 134 \quad a_{i+\frac{1}{2}}^- = \min \left[ \lambda_1 \left( q_{i+\frac{1}{2}}^- \right), \lambda_1 \left( q_{i+\frac{1}{2}}^+ \right), 0 \right]$$

135 and

$$136 \quad 137 \quad a_{i+\frac{1}{2}}^+ = \max \left[ \lambda_2 \left( q_{i+\frac{1}{2}}^- \right), \lambda_2 \left( q_{i+\frac{1}{2}}^+ \right), 0 \right]$$

138 where  $\lambda_1$  and  $\lambda_2$  are estimates of the smallest and largest eigenvalues respectively of the  
 139 Jacobian,  $\partial f / \partial u$ .

#### 140 Propagation Speeds of a Local Shock

141 As demonstrated in Zoppou (2014)  $\lambda_1$  and  $\lambda_2$  are bounded by the phase speed of the  
 142 shallow water wave equations, so that

$$143 \quad \lambda_1 := u - \sqrt{gh} \leq v_p \leq u + \sqrt{gh} =: \lambda_2$$

144 where  $v_p$  is the phase speed of the Serre equations, thus  $a_{i+1/2}^-$  and  $a_{i+1/2}^+$  are fully deter-  
 145 mined.

#### 146 Reconstruction

147 The quantities  $q_{i+1/2}^-$  and  $q_{i+1/2}^+$  in (7) are given by the two reconstructions at  $x_{i+1/2}$ ,  
 148 one from the cell to the left  $[x_{i-1/2}, x_{i+1/2}]$  and one from the cell to the right  $[x_{i+1/2}, x_{i+3/2}]$   
 149 denoted by the superscripts  $-$  and  $+$  respectively. The order of the polynomials used to  
 150 reconstruct the quantities inside the cells determines the spatial order of accuracy. Constant  
 151 polynomials result in a first-order method (Godunov 1959). Similarly first- and second-  
 152 degree polynomials result in second- and third-order accurate methods respectively.

153 For a zero-degree polynomial the interpolant has the value  $\bar{q}_i$  at  $x_i$ , this is also the  
 154 case for linear interpolation functions. For the zero-degree case the interpolants are fully  
 155 determined i.e  $q_{i-1/2}^+ = \bar{q}_i = q_{i+1/2}^-$  and monotonicity preserving. There are a variety of  
 156 ways to construct higher-degree interpolants not all of which are necessarily monotonicity  
 157 preserving, which can result in the introduction of numerical oscillations during the re-  
 158 construction process. To suppress these non-physical oscillations in higher order methods  
 159 limiting must be implemented. For the second-order method the minmod limiter was used  
 160 as in Kurganov et al. (2002). While for the third-order method the Koren limiter was used  
 161 (Koren 1993). This results in the following reconstruction scheme for the second-order  
 162 method

$$164 \quad 165 \quad q_{i+\frac{1}{2}}^- = \bar{q}_i + a_i \frac{\Delta x}{2}$$

166 and

167                   168

$$q_{i+\frac{1}{2}}^+ = \bar{q}_{i+1} - a_{i+1} \frac{\Delta x}{2}$$

169 where

170                   171

$$a_i = \text{minmod} \left\{ \theta \frac{\bar{q}_{i+1} - \bar{q}_i}{\Delta x}, \frac{\bar{q}_{i+1} - \bar{q}_{i-1}}{2\Delta x}, \theta \frac{\bar{q}_i - \bar{q}_{i-1}}{\Delta x} \right\} \quad \text{for } \theta \in [1, 2].$$

172 While for the third-order method the reconstruction scheme is

173                   174

$$q_{i+\frac{1}{2}}^- = \bar{q}_i + \frac{1}{2} \phi^-(r_i) (\bar{q}_i - \bar{q}_{i-1})$$

175 and

176                   177

$$q_{i+\frac{1}{2}}^+ = \bar{q}_{i+1} - \frac{1}{2} \phi^+(r_{i+1}) (\bar{q}_{i+1} - \bar{q}_i)$$

178 where

179                   180

$$\phi^-(r_i) = \max \left[ 0, \min \left[ 2r_i, \frac{1+2r_i}{3}, 2 \right] \right],$$

182                   183

$$\phi^+(r_i) = \max \left[ 0, \min \left[ 2r_i, \frac{2+r_i}{3}, 2 \right] \right]$$

184 and

185                   186

$$r_i = \frac{\bar{q}_{i+1} - \bar{q}_i}{\bar{q}_i - \bar{q}_{i-1}}.$$

187 **Fully discrete approximations to the instantaneous flux  $f(q_{i+\frac{1}{2}}^\pm)$**

188 For water depth, the fully discrete approximation to  $f(h_{i+1/2}^\pm)$  in (3a) is given by

189                   190

$$f\left(h_{i+\frac{1}{2}}^\pm\right) = u_{i+\frac{1}{2}}^\pm h_{i+\frac{1}{2}}^\pm$$

191 which is independent of the order of accuracy of the method.

192 The flux  $f(G_{i+1/2}^\pm)$  is more complicated because of the derivative term in (3b) and is  
193 given by

194                   195

$$f\left(G_{i+\frac{1}{2}}^\pm\right) = u_{i+\frac{1}{2}}^\pm G_{i+\frac{1}{2}}^\pm + \frac{g\left(h_{i+\frac{1}{2}}^\pm\right)^2}{2} - \frac{2\left(h_{i+\frac{1}{2}}^\pm\right)^3}{3} \left[ \left( \frac{\partial u}{\partial x} \right)_{i+\frac{1}{2}}^\pm \right]^2.$$

196 The first- and third-order approximations to the derivative term can be obtained by an  
 197 upwind finite difference approximation. By assuming that  $u$  is continuous, a second-order  
 198 approximation that has the correct order and is simpler to implement than its corresponding  
 199 upwind finite difference approximation can be used. Thus the following approximations  
 200 to the derivatives were obtained, for the first-order method

$$201 \quad \left( \frac{\partial u}{\partial x} \right)_{i+\frac{1}{2}}^+ = \frac{u_{i+\frac{3}{2}}^+ - u_{i+\frac{1}{2}}^+}{\Delta x}$$

$$202$$

203 and

$$204 \quad \left( \frac{\partial u}{\partial x} \right)_{i+\frac{1}{2}}^- = \frac{u_{i+\frac{1}{2}}^- - u_{i-\frac{1}{2}}^-}{\Delta x}.$$

$$205$$

206 For the second-order method

$$207 \quad \left( \frac{\partial u}{\partial x} \right)_{i+\frac{1}{2}}^- = \left( \frac{\partial u}{\partial x} \right)_{i+\frac{1}{2}}^+ = \frac{u_{i+1} - u_i}{\Delta x}$$

$$208$$

209 and for the third-order method

$$210 \quad \left( \frac{\partial u}{\partial x} \right)_{i+\frac{1}{2}}^+ = \frac{-u_{i+\frac{5}{2}}^+ + 4u_{i+\frac{3}{2}}^+ - 3u_{i+\frac{1}{2}}^+}{\Delta x}$$

$$211$$

212 and

$$213 \quad \left( \frac{\partial u}{\partial x} \right)_{i+\frac{1}{2}}^- = \frac{3u_{i+\frac{1}{2}}^- - 4u_{i-\frac{1}{2}}^- + u_{i-\frac{3}{2}}^-}{\Delta x}.$$

$$214$$

## 215 Transforming between nodal values and cell averages

216 The operator  $\mathcal{L}$  given by (6) uses cell averages while the operator  $\mathcal{A}$  given by (5a)  
 217 and (5b) uses nodal values at the cell centres. Therefore, a transformation from the cell  
 218 averages to the nodal values is required. For the first- and second-order methods this  
 219 distinction is trivial since  $\bar{q}_i = q_i$ . However, for the third-order method this is a very  
 220 important distinction and failure to handle this correctly will result in a loss of accuracy.

221 A quadratic polynomial that gives the correct cell averages for the cell centred at  $x_i$   
 222 and its two neighbours satisfies this equation

$$223 \quad q_i = \frac{-\bar{q}_{i+1} + 26\bar{q}_i - \bar{q}_{i-1}}{24}.$$

$$224$$

225 This is a tri-diagonal matrix equation that transforms from cell averages to nodal values  
 226 with third-order accuracy and is denoted by  $\mathcal{M}$ . The inverse transformation  $\mathcal{M}^{-1}$  denotes  
 227 the solution of the tri-diagonal matrix equation given nodal values resulting in cell aver-  
 228 ages which is also third-order accurate. For the first- and second-order schemes  $\mathcal{M}$  is the  
 229 identity matrix. This completes the solution of the Serre equations (2) and (3) with the  
 230 following process denoted by  $\mathcal{H}$

231

$$\mathcal{H}(\bar{\mathbf{U}}^n, \Delta t) = \begin{cases} \mathbf{U}^n &= \mathcal{M}(\bar{\mathbf{U}}^n) \\ \mathbf{u}^n &= \mathcal{A}(\mathbf{U}^n) \\ \bar{\mathbf{u}}^n &= \mathcal{M}^{-1}(\mathbf{u}^n) \\ \bar{\mathbf{U}}^{n+1} &= \mathcal{L}(\bar{\mathbf{U}}^n, \bar{\mathbf{u}}^n, \Delta t) \end{cases}.$$

232

233 **Strong-Stability-Preserving Runge-Kutta Scheme**

234 The process above is first-order accurate in time. This paper will use the strong sta-  
 235 bility Runge-Kutta steps described in Gottlieb et al. (2009) to construct fully second- and  
 236 third-order accurate methods using linear combinations of  $\mathcal{H}$ . This leads to the following  
 237 processes, for the first-order method

238

$$\bar{\mathbf{U}}^{n+1} = \mathcal{H}(\bar{\mathbf{U}}^n, \Delta t)$$

239

240 the second-order method

241

$$\bar{\mathbf{U}}^{(1)} = \mathcal{H}(\bar{\mathbf{U}}^n, \Delta t),$$

242

$$\bar{\mathbf{U}}^{(2)} = \mathcal{H}(\bar{\mathbf{U}}^{(1)}, \Delta t),$$

243

$$\bar{\mathbf{U}}^{n+1} = \frac{1}{2}(\bar{\mathbf{U}}^{(1)} + \bar{\mathbf{U}}^{(2)})$$

244

245 and the third-order method

246

$$\bar{\mathbf{U}}^{(1)} = \mathcal{H}(\bar{\mathbf{U}}^n, \Delta t),$$

247

$$\bar{\mathbf{U}}^{(2)} = \mathcal{H}(\bar{\mathbf{U}}^{(1)}, \Delta t),$$

248

$$\bar{\mathbf{U}}^{(3)} = \frac{3}{4}\bar{\mathbf{U}}^n + \frac{1}{4}\bar{\mathbf{U}}^{(2)},$$

249

$$\bar{\mathbf{U}}^{(4)} = \mathcal{H}(\bar{\mathbf{U}}^{(3)}, \Delta t),$$

250

$$\bar{\mathbf{U}}^{n+1} = \frac{1}{3}\bar{\mathbf{U}}^n + \frac{2}{3}\bar{\mathbf{U}}^{(4)}.$$

251

252 **Stability Constraint**

253 A necessary condition for stability of all these explicit methods based on the finite  
 254 volume method is the Courant-Friedrichs-Lowy condition (Courant et al. 1928) which  
 255 states that for each cell

256 
$$\Delta t < \frac{\Delta x}{2 \max(|\lambda_i|)} \forall i. \quad (8)$$

257

258

259 **NUMERICAL SIMULATIONS**

260 The discussed methods will now be used to solve three different problems; (i) the  
 261 soliton which is an analytic solution of the Serre equations; (ii) one of the experiments  
 262 conducted by Hammack and Segur (1978) and (iii) a dam-break problem from El et al.  
 263 (2006) and Le Métayer et al. (2010). The first two will be used to validate the models,  
 264 with the soliton used to confirm the order of convergence of the models. The second  
 265 problem is used to validate the models using experimental data which contains flows with  
 266 steep gradients. Lastly the dam-break problem will be used to compare the results of these  
 267 methods with those of El et al. (2006) and Le Métayer et al. (2010). The aim of which is to  
 268 verify the claim of the latter that a first-order method for the Serre equations is sufficiently  
 269 accurate to capture the important behaviour of the dam-break problem.

270 **Soliton**

271 Currently cnoidal waves are the only family of analytic solutions to the Serre equa-  
 272 tions (Carter and Cienfuegos 2011). Solitons are a particular instance of cnoidal waves  
 273 that travel without deformation and have been used to verify the convergence rates of the  
 274 proposed methods in this paper.

275 For the Serre equations the solitons have the following form

276 
$$h(x, t) = a_0 + a_1 \operatorname{sech}^2(\kappa(x - ct)) \quad (9a)$$

and

$$u(x, t) = c \left( 1 - \frac{a_0}{h(x, t)} \right) \quad (9b)$$

where

$$\kappa = \frac{\sqrt{3a_1}}{2a_0 \sqrt{a_0 + a_1}} \quad (9c)$$

278 and

$$c = \sqrt{g(a_0 + a_1)} \quad (9d)$$

279 where  $a_0$  and  $a_1$  are input parameters that determine the depth of the quiescent water and  
280 the maximum height of the soliton above that respectively. In the simulation  $a_0 = 10\text{m}$ ,  
281  $a_1 = 1\text{m}$  for  $x \in [-500\text{m}, 1500\text{m}]$  and  $t \in [0\text{s}, 100\text{s}]$ . With  $\Delta t = 0.01\Delta x$  which satisfies (8)  
282 and  $\theta = 1.2$  for the second-order reconstruction. The example results for  $\Delta x = 100/2^6\text{m}$   
283 can be seen in Figure 2.

284 Figure 2 demonstrates the superiority of the second- and third-order methods compared  
285 to the first-order method. With the first-order method there is significant attenuation of the  
286 wave due to its diffusive behaviour which creates a wider wave profile and some smaller  
287 trailing waves. However, the first-order method does produce the correct speed of the  
288 wave with a small phase error. While the second- and third-order methods demonstrate no  
289 noticeable deformation resolving the soliton solution well on a relatively coarse grid with  
290 less than 500 cells defining the actual wave.

291 The relative error as measured by the  $L_1$ -norm of the method can be seen in Figure 3.  
292 For a vector  $\mathbf{q}$  and an approximation to it  $\mathbf{q}^*$  the relative error as measured by the  $L_1$ -norm  
293 is

$$294 \quad L_1(\mathbf{q}, \mathbf{q}^*) = \frac{\sum_{i=1}^m |q_i - q_i^*|}{\sum_{i=1}^m |q_i|}.$$

296 Figure 3 demonstrates that the methods all have the correct order of convergence in  
297 both time and space. However, this order of convergence is not uniform over all  $\Delta x$ . When  
298  $\Delta x$  is large the actual problem is not discretised well since the cells are too large to ade-  
299 quately resolve the problem; this causes the observed suboptimal rate of convergence in  
300 Figure 3. When  $\Delta x$  is sufficiently small the numerical errors become small enough that  
301 floating point errors are significant and this can also lead to suboptimal rates of conver-  
302 gence as can be seen in the relative errors for the third-order method using the same initial  
303 conditions and parameters with  $t \in [0, 1\text{s}]$  in Figure [ ]. Thus the suboptimal rates for  
304 the third-order method in Figure 3(c) at small  $\Delta x$  are the result of floating point errors.  
305 Therefore, the order of convergence for all methods is confirmed.

306 Figure 3 also demonstrates the superiority of the second- and third-order methods over  
307 the first-order method for accuracy. The third-order method is also better than the second-  
308 order method in this respect although this difference is less pronounced. These differences  
309 have a significant impact on run-time if one wishes to run a simulation up to a desired  
310 accuracy. A comparison of the methods for such a problem is presented in Table 1.

311 The first-order method has a runtime two orders of magnitude greater than the second-  
312 and third-order methods. Which is reasonable because the difference in  $\Delta x$  is also two

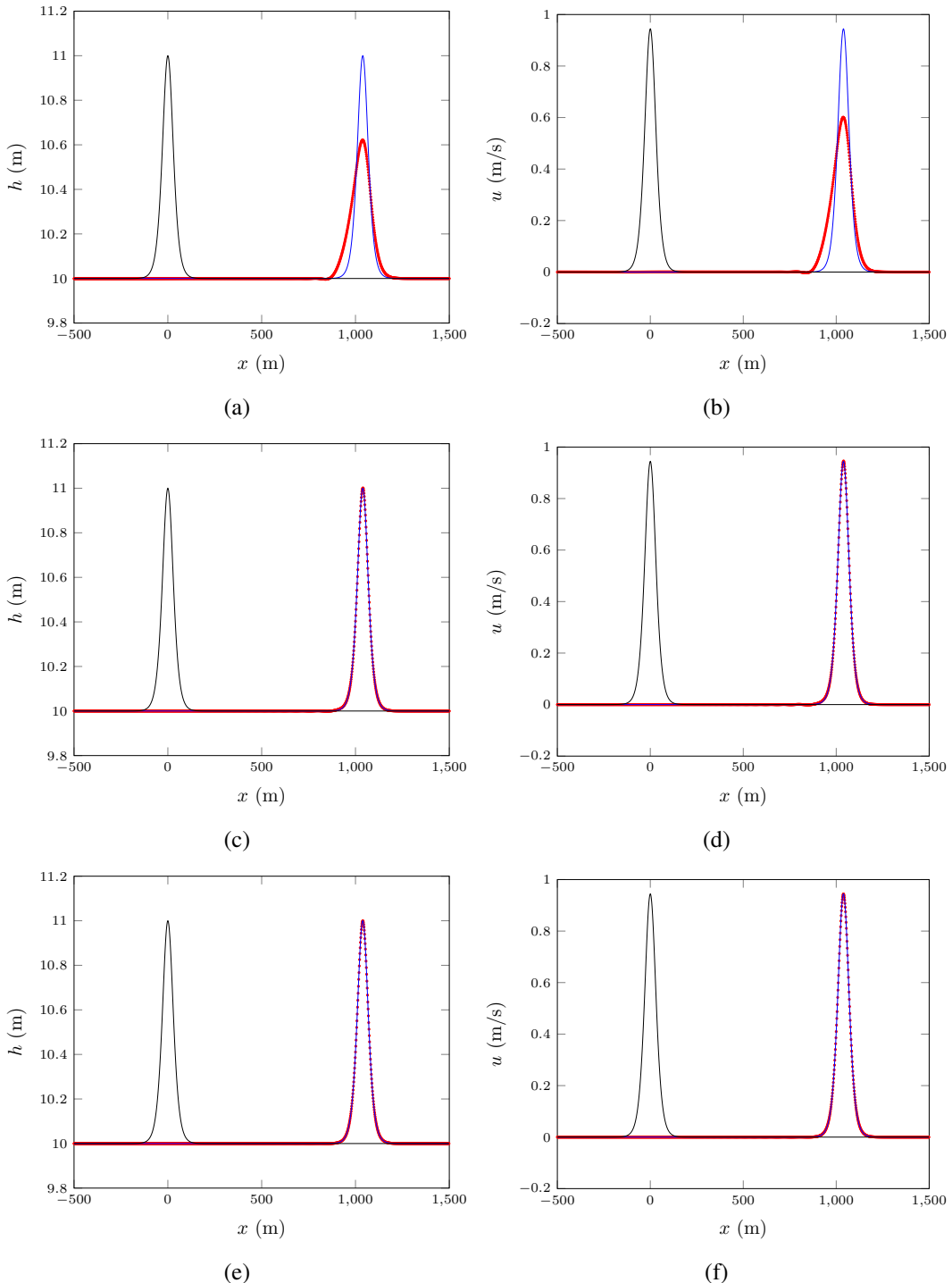


FIG. 2: The first-, second- and third-order simulation of a soliton with  $\Delta x = 100/2^6$ m (●) plotted against the analytic solution of (9) (—) with black for  $t = 0$ s and blue for  $t = 100$ s.

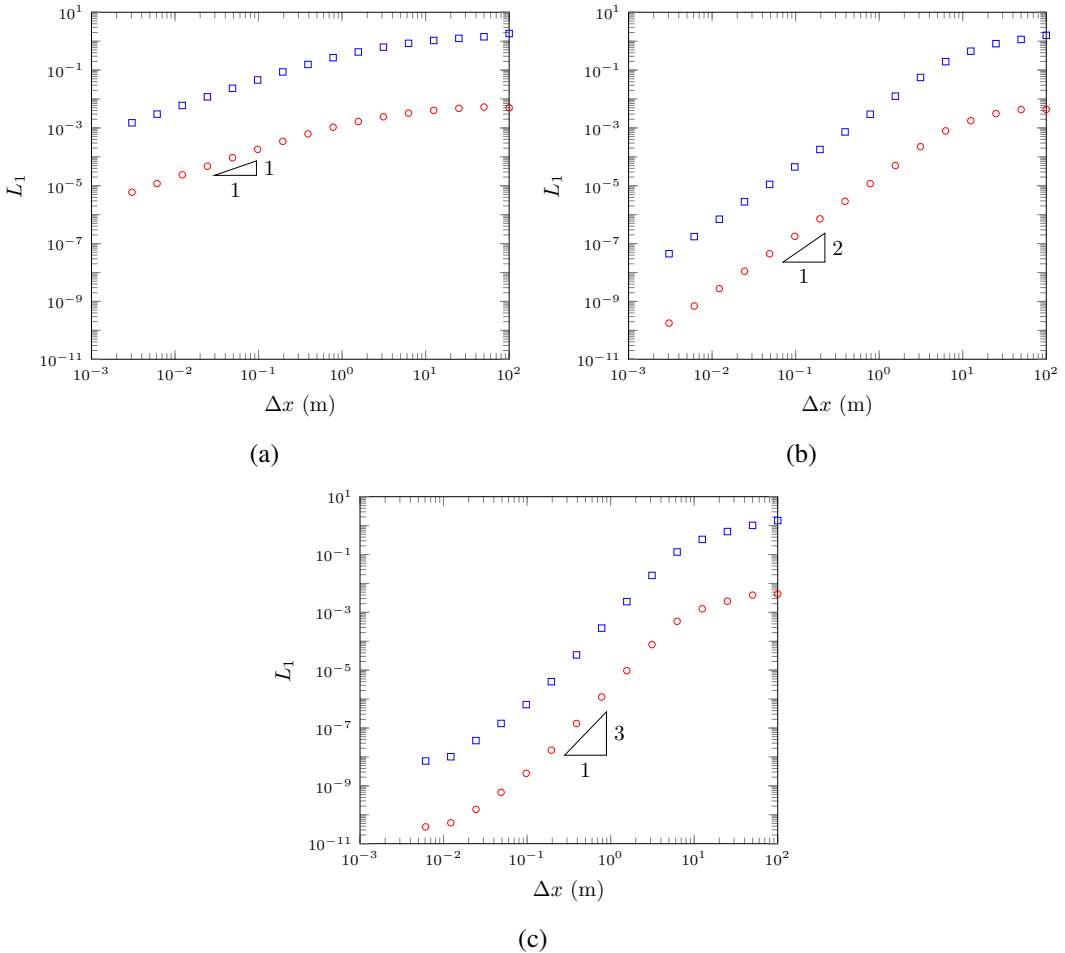


FIG. 3: Convergence of relative error using  $L_1$  norm for analytic soliton solution for both  $h$  ( $\circ$ ) and  $u$  ( $\diamond$ ) for the; (a) first-, (b) second- and (c) third-order methods.

orders of magnitude. This is computationally restrictive as running practical problems to a reasonable accuracy can have run times that are excessive compared to second- and third-order accurate schemes. Although the second- and third-order methods are more computationally complex than the first-order method this complexity is justified if one wants to numerically solve the Serre equations up to some desired accuracy. This also demonstrates that the second-order method is adequate compared to the third-order method for solving the Serre equations up to some desired accuracy.

Figure 3(b) and Figure 3(c) demonstrate that the second- and third-order methods both have similar errors and Figure 2 shows that these methods resolve the problem well. There-

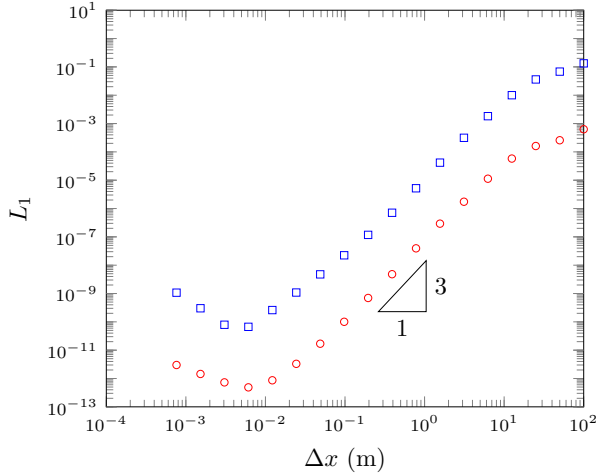


FIG. 4: Convergence of relative error using  $L_1$  norm for analytic soliton solution for both  $h$  ( $\circ$ ) and  $u$  ( $\diamond$ ) over only a single time step

Order	$\Delta x$ (m)	$L_1$ relative error for $h$	$L_1$ relative error for $u$	Run Time (s)
First	$100/2^{11}$	$9.32715378271 \times 10^{-5}$	$2.34320597345 \times 10^{-2}$	481.216886997
Second	$100/2^6$	$5.00595847273 \times 10^{-5}$	$1.25175521776 \times 10^{-2}$	2.19665694237
Third	$100/2^5$	$7.681432554 \times 10^{-5}$	$1.89115440455 \times 10^{-2}$	1.3766579628

TABLE 1: Comparison of run times for different order methods to get similar relative error as measured by the  $L_1$  norm for  $h$

fore, the extra effort in running a third-order method compared to a second-order method is not justified in this case. While the effort required to go from a first-order method to a second-order method is justified since attaining a similar accuracy between them requires a restrictively small  $\Delta x$  for a first-order method.

### Segur Laboratory Experiment

Hammack and Segur (1978) conducted an experiment that produced rectangular waves with the stroke of a 0.61m long piston flush with the wall of a wave tank 31.6m in length. The water height was recorded at 0m, 5m, 10m, 15m and 20m from the edge of the piston furthest from the wall over time. The quiescent water height  $h_1$  was 0.1m while the stroke of the piston caused a depression of water which was  $h_0 = 0.095$ m deep. To run this as a numerical simulation the reflected problem was used. Thus the initial conditions were reflected around the origin and  $h_1 - h_0$  was doubled by setting  $h_0 = 0.09$ m. The domain was chosen to be from  $-60$ m to  $60$ m and the simulation was for  $t \in [0\text{s}, 50\text{s}]$  with  $\Delta x = 0.01\text{m}$ ,  $\lambda = 0.2 / \sqrt{gh_1}$  m/s which satisfies (8) and  $\theta = 1.2$  in the second-order scheme. The results

336 of this simulation are displayed in Figures 5 - 7.

337 In this experiment for the positive side of the axis the initial depression causes a right  
338 going rarefaction fan and a left going shock. The shocks from both sides then reflect at  
339 the origin and so the shock and the rarefaction fan will travel in the same direction. The  
340 leading wave in all the related figures is the rarefaction fan while the trailing dispersive  
341 waves are the result of the reflected shock.

342 From all the related figures it can be seen that all models show good agreement be-  
343 tween the arrival of the first wave and the period of all the waves. While Figure 5 shows  
344 the first-order method is too diffusive and thus under estimates the heights of the dispersive  
345 waves. Whereas the second- and third-order methods over estimate them. This overesti-  
346 mation can be explained by the Serre equations ignoring viscous effects that may diffuse  
347 the dispersive waves and so the results could be considered as an upper bound on the wave  
348 heights for non-inviscid fluids. Although even without these effects these numerical meth-  
349 ods show good agreement with the experimental data thus validating them to provide a  
350 reasonable representation of rapidly-varying flows. Additionally, it demonstrates that the  
351 oscillations observed by the produced numerical solutions of the Serre equations around  
352 steep gradients are physical and not numerical. In these simulations the numerical oscil-  
353 lations that the second-order method should produce (Zoppou and Roberts 1996) do not  
354 have a significant influence on the physical oscillations.

### 355 Dam-Break

356 The dam-break problem used by El et al. (2006) to compare their analysis with a  
357 second-order accurate solution of the Serre equations can be defined by

$$358 h(x, 0) = \begin{cases} 1.8m & x < 500m \\ 1.0m & x \geq 500m \end{cases},$$

$$359 u(x, 0) = 0.0m/s.$$

360 With  $x \in [0m, 1000m]$  for  $t \in [0s, 30s]$ . Where  $\lambda = 0.01m/s$  which satisfies (8) and  $\theta = 1.2$   
361 for the second-order scheme. This corresponds to sub-critical flow and was a situation  
362 demonstrated in El et al. (2006) and Le Métayer et al. (2010). An example was plotted  
363 for  $\Delta x = 100/2^{10}m$  for all the methods and for  $\Delta x = 100/2^{15}m$  for the first-order method  
364 in Figure 9. To determine if the oscillations that occur in the solution indeed converge  
365 to some limit as  $\Delta x \rightarrow 0$  multiple  $\Delta x$  values were run and then the amount of variation  
366 in the solution measured. This measured how oscillatory the solution was and was used  
367 to determine the growth of the oscillations. A common way to measure this is the total  
368 variation (TV) which for  $\mathbf{q}$  is given by

$$369 TV(\mathbf{q}) = \sum_{\forall i>1} |q_i - q_{i-1}|.$$

370

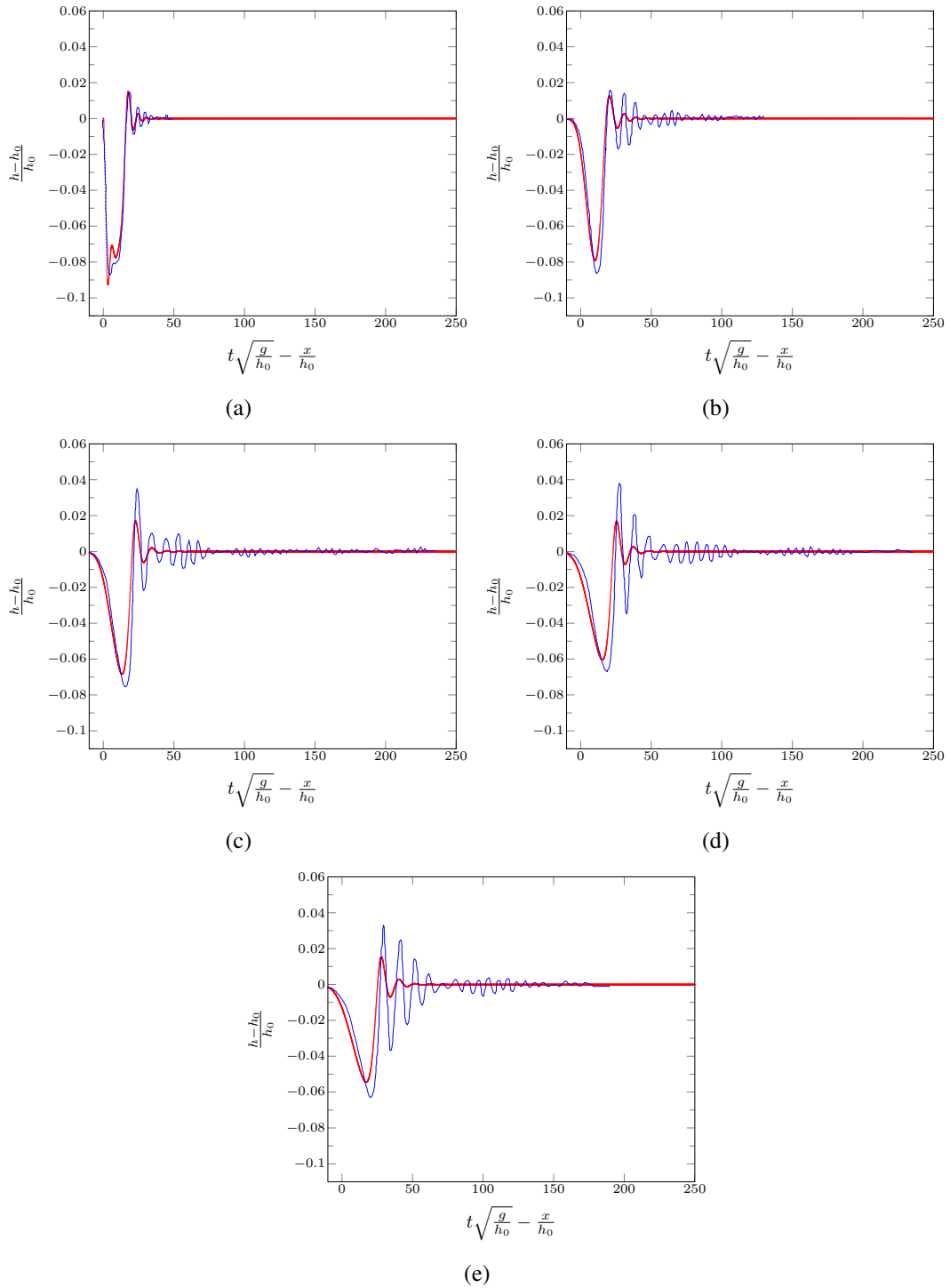


FIG. 5: Comparison of the experimental results (—) against the first-order methods solution (●) at  $x/h_0$  : (a) 0, (b) 50, (c) 100, (d) 150 and (e) 200.

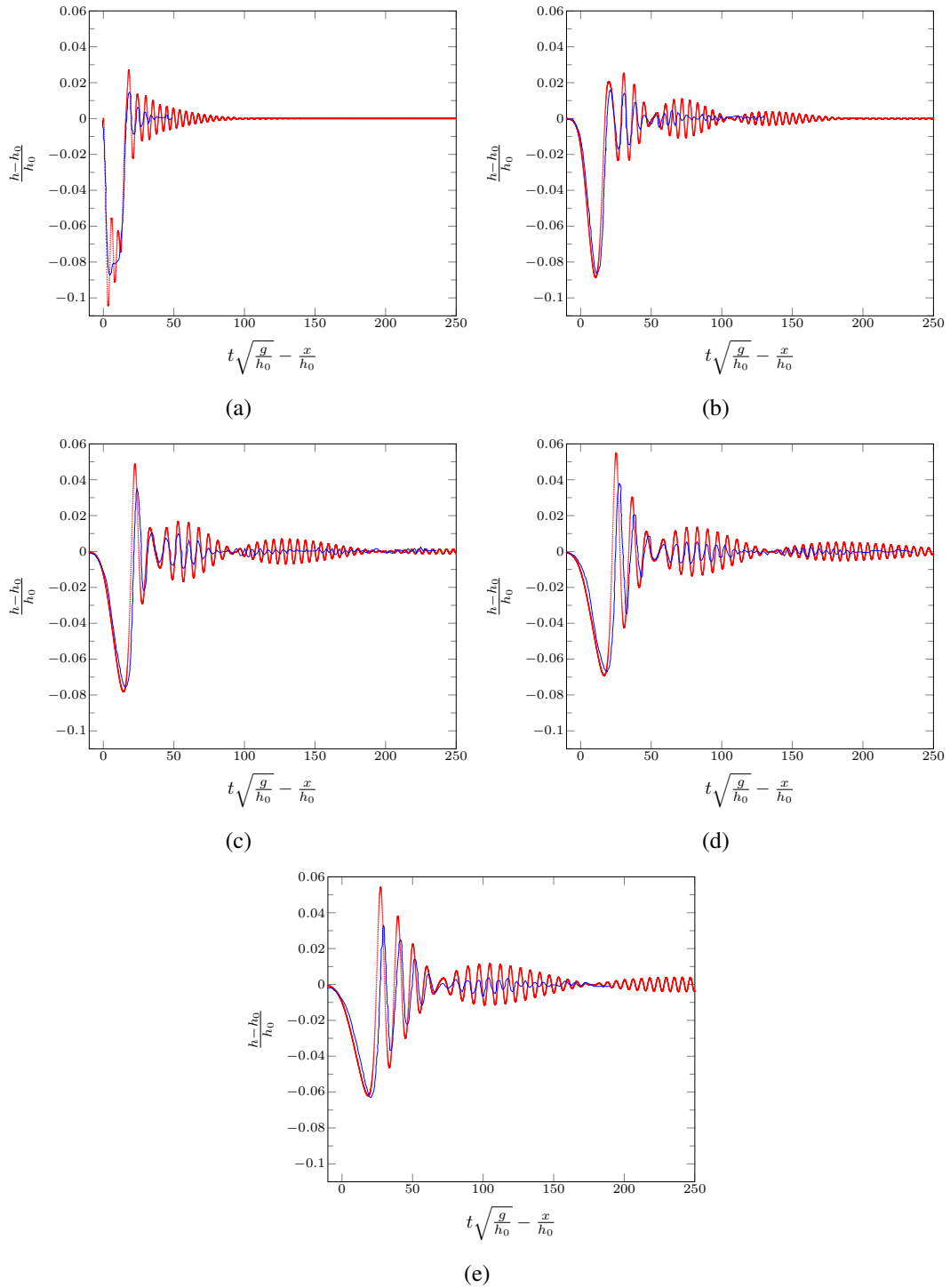


FIG. 6: Comparison of the experimental results (—) against the second-order methods solution (●) at  $x/h_0$  : (a) 0, (b) 50, (c) 100, (d) 150 and (e) 200.

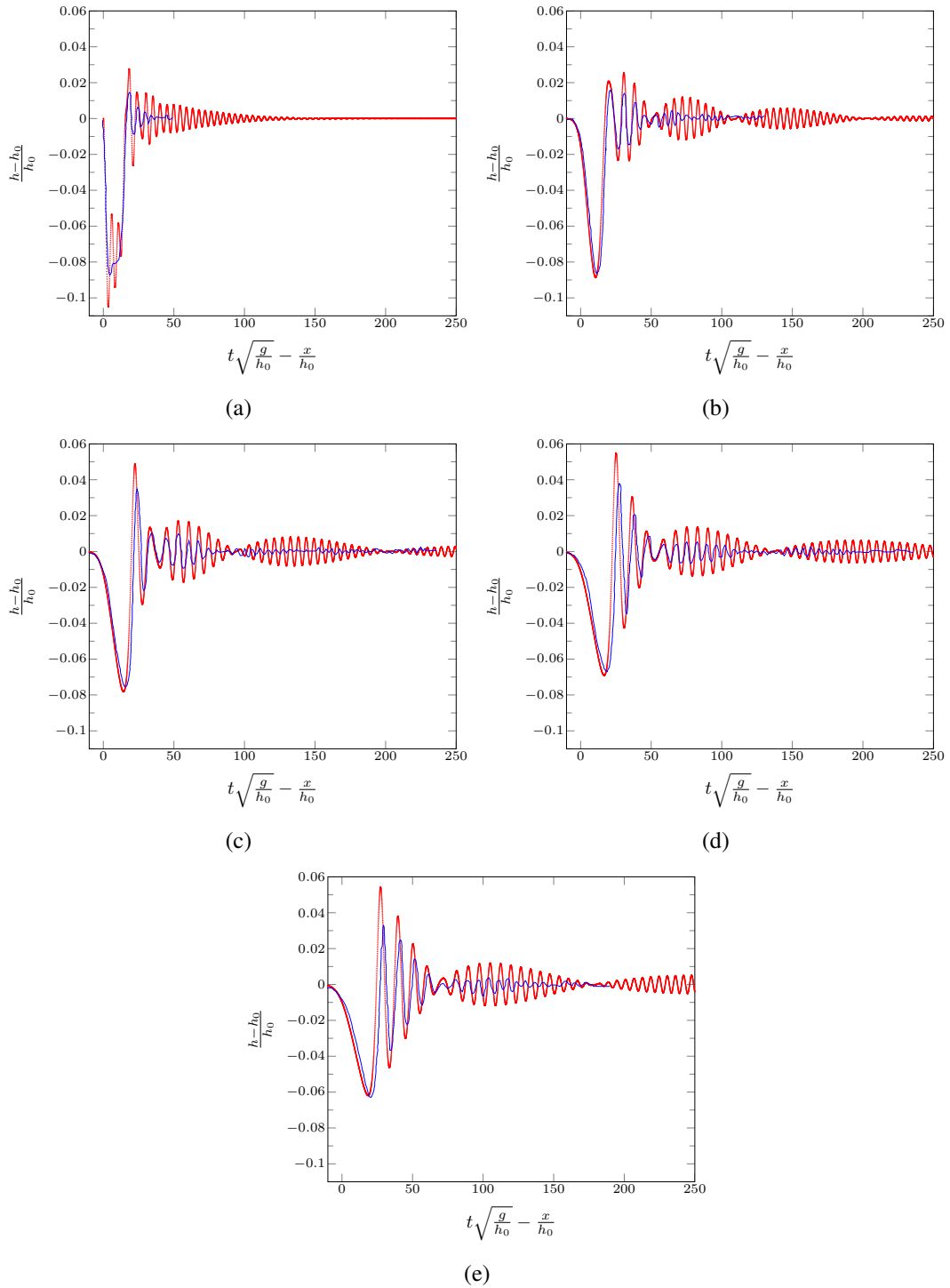


FIG. 7: Comparison of the experimental results (—) against the third-order methods solution (●) at  $x/h_0$  : (a) 0, (b) 50, (c) 100, (d) 150 and (e) 200.

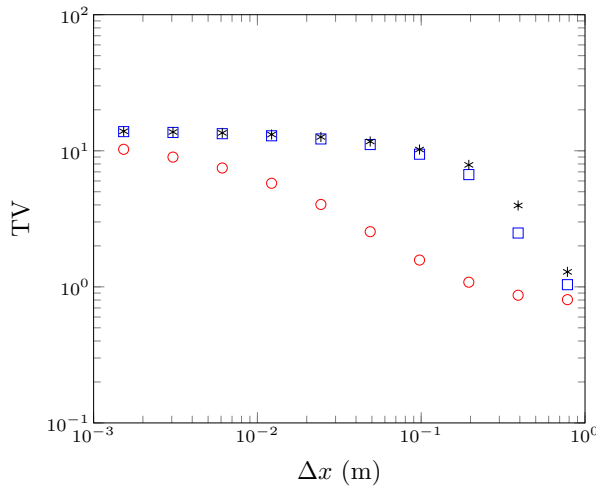


FIG. 8: The change in total variation (TV) over  $\Delta x$  for; (○) first-, (□) second-, and (\*) third-order methods.

If the solution does indeed converge then the TV must at some point plateau, bounding the oscillations. This was indeed the findings of the experiments as can be seen by Figure 8. The TV increases as  $\Delta x$  decreased because the models resolved more dispersive waves. As  $\Delta x$  decreased further the TV plateaued and so the size and number of oscillations was bounded. Therefore, the method has not become unstable which supports the argument that the numerical methods do not introduce non-physical oscillations in the solution. Under this measure the second-order method converges rapidly to the solution of the third-order method.

These solutions compare very well to the findings in El et al. (2006) with both the second- and third-order methods resolving the oscillations around the “contact discontinuity”(El et al. 2006) between the rarefaction fan and the shock. In Le Métayer et al. (2010) it was reported that for their first-order method such oscillatory behaviour was not seen. However, for the first-order method proposed in this paper when  $\Delta x = 100/2^{15}$  it was resolved as in Figure 9(d). This validates the findings in El et al. (2006). Interestingly this is a much higher resolution than one needs to represent the waves themselves. It appears that the behaviour of the dispersive waves around a steep gradient is sensitive to diffusion so that even though the first-order method in Figure 9(a) heuristically had enough cells to resolve most of the wave train, due to strong diffusion hardly any of the wave train was resolved.

There is a good agreement between the second- and third-order simulations of the dam-

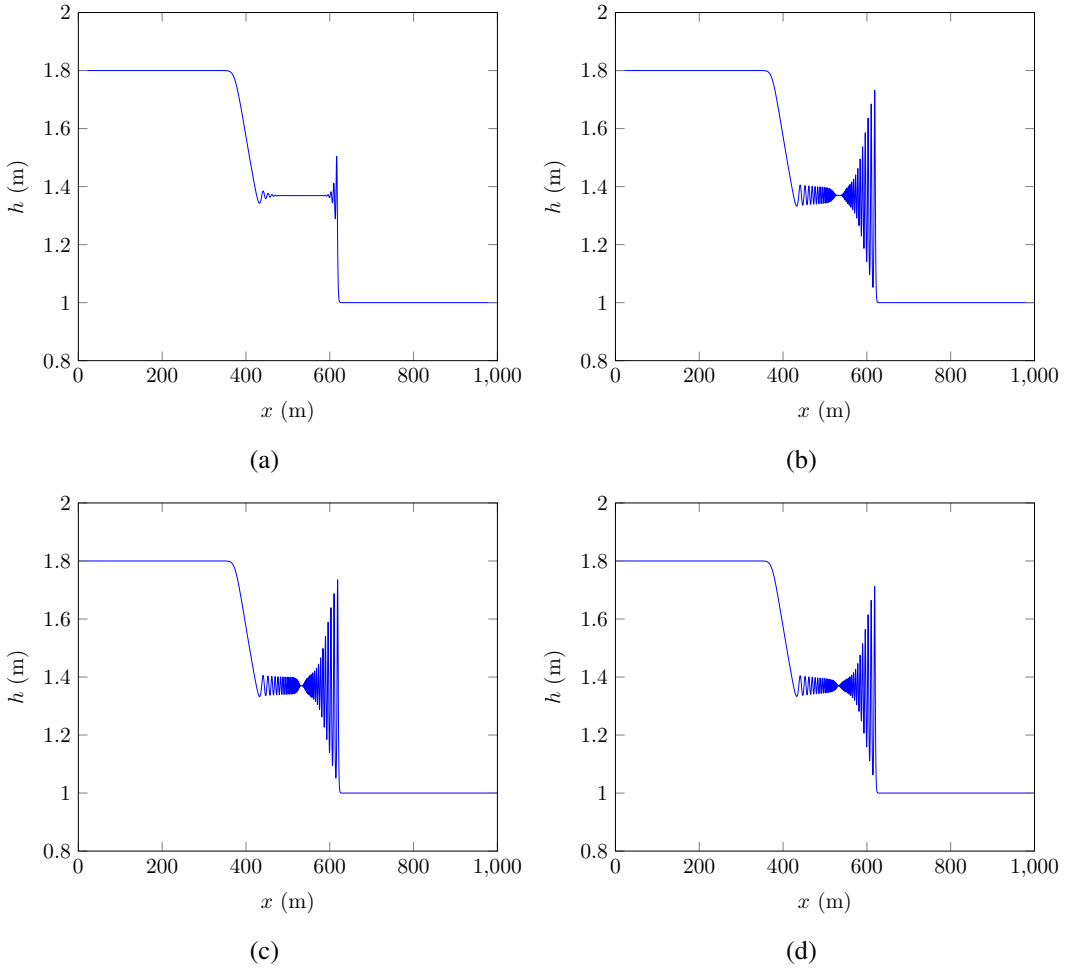


FIG. 9: Solution of the dam-break problem using the (a) first-, (b) second- and (c) third-order method with  $\Delta x = 100/2^{10}$ m. As well as a (d) first-order method with  $\Delta x = 100/2^{15}$ m.

break problem as can be seen in Figures 9(b) and 9(c). Although more oscillations are resolved by the third-order method over the second-order method, there is no significant change in the resolved behaviour of this problem between the two methods. As noted in the introduction second-order accurate numerical schemes are dissipative; since the diffusive third-order method resolved the same oscillations it was demonstrated that none of the dissipative errors significantly polluted the wave train and for this problem the second-order accurate scheme is capable of resolving the problem.

398 **CONCLUSIONS**

399 First-, second- and third-order hybrid finite difference-volume methods were devel-  
400 oped to solve the Serre equations written in conservative law form. The methods were  
401 then tested and validated. Firstly the order of the methods were all verified, secondly  
402 the methods steep gradient handling capability was validated by comparison with experi-  
403 mental data. Thirdly the behaviour of the solutions matched previous findings in El et al.  
404 (2006). Thus it can be concluded that these methods are all valid and they properly handle  
405 steep gradients. It was also demonstrated that for these equations although second-order  
406 is not as accurate as third-order it still provides a satisfactory method for reasonable  $\Delta x$   
407 unlike the first-order method which due to the introduction of large numerical diffusion  
408 requires computationally restrictive  $\Delta x$  to produce satisfactory accuracy. Therefore; prac-  
409 tical problems which contain steep gradients require at least a second-order method to  
410 solve the Serre equations.

411 **ACKNOWLEDGEMENTS**

412 Dr David George, Cascades Volcano Observatory, U.S. Geological Survey for providing  
413 the rectangular wave data.

414 **REFERENCES**

- 415 Antunes do Carmo, A., Seabra-Santos, F. J., and Almeida, A. B. (1993). “Numerical solution  
416 of the generalized Serre equations with the MacCormack finite-difference scheme.” *International Journal for Numerical Methods in Fluids*, 16(8), 725–738.
- 417 Bonneton, P., Chazel, F., Lannes, D., Marche, F., and Tissier, M. (2011). “A splitting approach for the fully nonlinear and weakly dispersive Green-Naghdi model.” *Journal of Computational Physics*, 230(4), 1479–1498.
- 418 Carter, J. D. and Cienfuegos, R. (2011). “Solitary and cnoidal wave solutions of the Serre  
419 equations and their stability.” *European Journal of Mechanics B/Fluids*, 30(3), 259–268.
- 420 Chazel, F., Lannes, D., and Marche, F. (2011). “Numerical simulation of strongly nonlinear  
421 and dispersive waves using a Green-Naghdi model.” *Journal of Scientific Computing*, 48(1-3), 105–116.
- 422 Cienfuegos, R. and Barthélemy, E. and Bonneton, P. (2006). “A fourth-order compact finite  
423 volume scheme for fully nonlinear and weakly dispersive Boussinesq-type equations.  
424 Part i: model development and analysis.” *International Journal for Numerical Methods  
425 in Fluids*, 51, 1217–1253.
- 426 Cienfuegos, R. and Barthélemy, E. and Bonneton, P. (2007). “A fourth-order compact finite  
427 volume scheme for fully nonlinear and weakly dispersive Boussinesq-type equations.  
428 Part ii: Boundary conditions and validation.” *International Journal for Numerical  
429 Methods in Fluids*, 53, 1423–1455.
- 430 Courant, R., Friedrichs, K., and Lewy, H. (1928). “Über die partiellen Differenzengleichungen  
431 der mathematischen physik.” *Mathematische Annalen*, 100(1), 32 – 74.
- 432 Dutykh, D., Clamond, D., Milewski, P., and Mitsotakis, D. (2011). “Finite volume and  
433 pseudo-spectral schemes for the fully nonlinear ‘irrotational’ Serre equations.” *Arxiv*,  
434 24(5), 0 – 25.
- 435 El, G., Grimshaw, R. H. J., and Smyth, N. F. (2006). “Unsteady undular bores in fully  
436 nonlinear shallow-water theory.” *Physics of Fluids*, 18(027104).
- 437 Godunov, S. K. (1959). “A difference method for numerical calculation of discontinuous  
438 solutions of the equations of hydrodynamics.” *Matematicheskii Sbornik*, 89(3), 271–  
439 306.
- 440 Gottlieb, S., Ketcheson, D. I., and Shu, C. W. (2009). “High order strong stability preserving  
441 time discretizations.” *Journal of Scientific Computing*, 38(3), 251–289.
- 442 Green, A. E. and Naghdi, P. M. (1976). “A derivation of equations for wave propagation  
443 in water of variable depth.” *Journal of Fluid Mechanics*, 78(2), 237–246.

- 448 Hammack, J. L. and Segur, H. (1978). “The Korteweg-de Vries equation and water waves.  
 449 Part 3. Oscillatory waves.” *Journal of Fluid Mechanics*, 84(2), 337–358.
- 450 Koren, B. (1993). “A robust upwind discretization method for advection, diffusion and  
 451 source terms.” *Notes on Numerical Fluid Mechanics*, Vol. 45, Centrum voor Wiskunde  
 452 en Informatica, Amsterdam.
- 453 Kurganov, A., Noelle, S., and Petrova, G. (2002). “Semidiscrete central-upwind schemes  
 454 for hyperbolic conservation laws and Hamilton-Jacobi equations.” *Journal of Scientific  
 455 Computing, Society for Industrial and Applied Mathematics*, 23(3), 707–740.
- 456 Lannes, D. and Bonneton, P. (2009). “*Physics of Fluids*, 21(1), 16601–16610.
- 457 Le Métayer, O., Gavrilyuk, S., and Hank, S. (2010). “A numerical scheme for the Green-  
 458 Naghdi model.” *Journal of Computational Physics*, 229(6), 2034–2045.
- 459 Li, M., Guyenne, P., Li, F., and Xu, L. (2014). “High order well-balanced CDG-FE meth-  
 460 ods for shallow water waves by a Green-Naghdi model.” *Journal of Computational  
 461 Physics*, 257, 169–192.
- 462 Mitsotakis, D., Ilan, B., and Dutykh, D. (2014). “On the Galerkin/Finite-Element Method  
 463 for the Serre Equations.” *Journal of Scientific Computing*, 61(1), 166–195.
- 464 Serre, F. (1953). “Contribution à l’étude des écoulements permanents et variables dans les  
 465 canaux.” *La Houille Blanche*, 6, 830–872.
- 466 Su, C. H. and Gardner, C. S. (1969). “Korteweg-de Vries equation and generalisations.  
 467 III. Derivation of the Korteweg-de Vries equation and Burgers equation.” *Journal of  
 468 Mathematical Physics*, 10(3), 536–539.
- 469 Zoppou, C. (2014). “Numerical solution of the One-dimensional and Cylindrical Serre  
 470 Equations for Rapidly Varying Free Surface Flows.” Ph.D. thesis, Australian National  
 471 University, Acton ACT 2601 Australia.
- 472 Zoppou, C. and Roberts, S. (1996). “Behaviour of finite difference schemes for advection  
 473 diffusion equations.” *Technical Report Mathematics Research Report No.MRR 062-96*.